Rapid Communications

Photogalvanic effect in Weyl semimetals from first principles

Yang Zhang,[1,2] Hiroaki Ishizuka,[3] Jeroen van den Brink,[2] Claudia Felser,[1] Binghai Yan,[4] and Naoto Nagaosa[3,5]
[1]*Max Planck Institute for Chemical Physics of Solids, 01187 Dresden, Germany*
[2]*Leibniz Institute for Solid State and Materials Research, 01069 Dresden, Germany*
[3]*Department of Applied Physics and Quantum Phase Electronics Center (QPEC), University of Tokyo, Tokyo 113-8656, Japan*
[4]*Department of Condensed Matter Physics, Weizmann Institute of Science, Rehovot 7610001, Israel*
[5]*RIKEN Center for Emergent Matter Science (CEMS), Wako 351-0198, Japan*

(Received 12 March 2018; published 29 June 2018)

Using first-principles calculations, we investigate the photogalvanic effect in the Weyl semimetal material TaAs. We find colossal photocurrents caused by the Weyl points in the band structure in a wide range of laser frequency. Our calculations reveal that the photocurrent is predominantly contributed by the three-band transition from the occupied Weyl band to the empty Weyl band via an intermediate band away from the Weyl cone, for excitations both by linearly and circularly polarized light. Therefore, it is essential to sum over all three-band transitions by considering a full set of Bloch bands (both Weyl bands and trivial bands) in the first-principles band structure while it does not suffice to only consider the two-band direct transition within a Weyl cone. The calculated photoconductivities are well consistent with recent experiment measurements. Our work provides a first-principles calculation on nonlinear optical phenomena of Weyl semimetals and provides a deeper understanding of the photogalvanic effects in complexed materials.

DOI: 10.1103/PhysRevB.97.241118

Introduction. Weyl fermions correspond to the massless solutions of the Dirac equation [1] and have been observed recently in solids as quasiparticles [2–6]. Related materials are called Weyl semimetals (WSMs) [7–13]. A WSM gives rise to linearly band-crossing points called Weyl points (WPs) in the momentum space. WPs are monopoles of the Berry curvature [14,15] with finite chirality and are related to the chiral anomaly in the context of high-energy physics [16–19] and unique surface Fermi arcs [2].

The monopole-type Berry curvature of WSMs can lead to appealing nonlinear optical effects that are intimately related to the Berry phase in the band structure [20–24]. Under strong light irradiation, an noncentrosymmetric material exhibits photocurrents as nonlinear functions of the electric field of the light and also generates higher harmonic frequencies, referred to as photogalvanic effects. The photogalvanic effect rectifies light to dc currents and often play a crucial role in optical devices and solar cells beyond the *p-n* junction platform [25–27]. Under linearly polarized light, the induced photocurrent is usually called a shift current that originates in the charge center shift between the valence and conduction bands in the optical excitation. Under circularly polarized light, the photocurrent generation is referred to as a circular photogalvanic effect (CPGE). It can be expressed in the formalism of the Berry curvature and Berry connection [22–24], revealing a topological nature. Therefore, WSMs have recently been theoretically investigated for such nonlinear optical phenomena [28–44]. In these works, two-band or four-band effective models are commonly adopted to reveal the relation between the photocurrent and the Weyl bands. For example, the tilt of the Weyl cones is proposed to play an essential role in generating a net CPGE current by considering the two-band transition from the occupied Weyl band to the empty Weyl band [39]. However, a first-principles investigation of the photogalvanic effects of WSMs, which accounts for the realistic material band structures, is still missing.

Recent experiments [45–50] have reported giant photocurrent effects and second-harmonic generation (SHG) in the TaAs-family WSMs exhibiting orders of magnitude larger responses than conventional nonlinear materials. However, some experiments seemingly contradict each other. Reference [46] reported a photocurrent caused by circularly polarized light, but claimed that a negligible photocurrent was caused by linearly polarized light through the shift current mechanism. In contrast, Ref. [48] reported a colossal shift current with linearly polarized light in the same compound. Therefore, accurate estimations of photocurrents are necessary and timely to identify quantitative contributions from the CPGE and shift current for a specific material. In addition, nonlinear optical phenomena are highly sensitive to the bulk Fermi surface topology but are insensitive to surface states. Hence, they can serve as a direct pathway to probe the topology inside the bulk.

In this Rapid Communication, we perform first-principles studies on the CPGE and shift current effect in WSMs. With the second-order Kubo formulism, we calculate the photocurrent conductivity in the inversion-asymmetric WSM TaAs via a multiband approach. Our results agree quantitatively with recent experiments. The shift current displays a close relation with the existence of WPs. Especially in the long-wavelength region, the shift current is predominantly contributed by virtual transitions from the occupied Weyl to the empty Weyl band through a third trivial band, referred to as the three-band transition, as illustrated in Fig. 1(b). For CPGE, three-band virtual transitions make the dominant contributions and are distributed relatively uniformly in the momentum space. In contrast, the two-band real transitions contribute much less

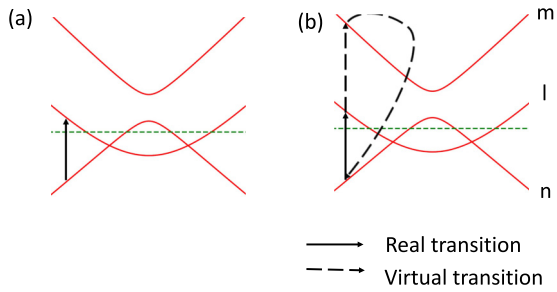

FIG. 1. Optical process for bands with a pair of Weyl nodes of (a) absorption and (b) dc photocurrent.

photocurrent, which is mainly caused by the Weyl cone regions. Given the significance of the three-band transitions, it is necessary to sum over all intermediate states by considering a full set of Bloch states. Then, the first-principles method is naturally the best way to compute the nonlinear response. For the same photon energy used in experiment, we find that the CPGE photocurrent is nearly two orders of magnitude greater than the shift current and clarify the possible reason why the shift current was not detected in a previous experiment that reported the CPGE [46].

Theory and method. The calculation of CPGE and shift current is based on a quadratic response theory proposed by von Baltz and Kraut [51–53], which accounts for a steady-state short-circuit photocurrent under linearly polarized light. To calculate the photocurrent also for circularly polarized light, we have generalized this quadratic response theory to a more general relation for the photoconductivity,

$$\sigma^c_{ab} = \frac{|e|^3}{8\pi^3\omega^2}\mathrm{Re}\left\{\phi_{ab}\sum_{\Omega=\pm\omega}\sum_{l,m,n}\int_{\mathrm{BZ}} d^3k(f_l - f_n) \times \frac{\langle n\vec{k}|\hat{v}_a|l\vec{k}\rangle\langle l\vec{k}|\hat{v}_b|m\vec{k}\rangle\langle m\vec{k}|\hat{v}_c|n\vec{k}\rangle}{(E_n - E_m - i\delta)(E_n - E_l + \hbar\Omega - i\delta)}\right\}. \quad (1)$$

The conductivity (σ^c_{ab}; $a,b,c = x,y,z$) is a third rank tensor and represents the photocurrent J^c generated by an electrical field $\vec{E}$ via $J^c = \sigma^c_{ab}E^*_a E_b$. Here, $\hat{v}_a = \frac{\hat{p}}{m_0}$, $E_n = E_n(\vec{k})$, and m_0, $\delta = \hbar/\tau$, τ stand for, respectively, the free-electron mass, broadening parameter, and the quasiparticle lifetime. ϕ_{ab} is the phase difference between the driving field $\vec{E}_a$ and $\vec{E}_b$, i.e., $\phi_{yz} = i$ for left-circularly polarized light propagating in the x direction with the light-polarization vector $(0,1,i)$. It is clear that the real part of the integral in Eq. (1) describes the shift current response under linearly polarized light and the imaginary part of the integral gives the helicity-dependent CPGE.

Next, we analyze the response tensor under time-reversal symmetry ($\hat{T}$) and point group symmetry. For simplicity, we define $N \equiv \langle n\vec{k}|\hat{v}_a|l\vec{k}\rangle\langle l\vec{k}|\hat{v}_b|m\vec{k}\rangle\langle m\vec{k}|\hat{v}_c|n\vec{k}\rangle$. $\hat{T}$ reverses the velocity and brings an additional minus sign to the imaginary part of N by a complex conjugation. Thus, in materials with time-reversal symmetry, the real part of the numerator is odd to $\vec{k}$ and therefore vanishes in the integral, and hence only the imaginary part of the numerator has to be taken into account for calculations on nonmagnetic WSMs. Since there is no current from $l = n$ or $m = n$, we can separate the contribution into two parts with respect to the band number l and m. The three-band processes ($n \to m \to l$) are given by $l \neq m$, and the two-band processes are given by $l = m$ (two-band transition). By applying point group symmetry operations to the numerator N, the third rank conductivity tensor shape can be determined, as can be the tensor form of the anomalous Hall conductivity and spin Hall conductivity [54,55].

To see the relations between the photocurrent response and the detailed band structure, we analyze the energy denominator by decomposing it into real and imaginary parts,

$$D_1 = \frac{1}{E_n - E_m - i\delta} = \frac{P}{E_n - E_m} + i\pi\delta(E_n - E_m),$$
$$D_2 = \frac{1}{E_n - E_l + \hbar\Omega - i\delta} = \frac{P}{E_n - E_l + \hbar\Omega} + i\pi\delta(E_n - E_l + \hbar\Omega). \quad (2)$$

Since the product of the three velocity matrices is purely imaginary, $\mathrm{Im}(D_1D_2)$ [$\sim\pi\frac{P}{(E_n-E_m)}\delta(E_n - E_l + \hbar\Omega)$] gives the shift current response when ϕ_{ab} is real. Only the momentum vector with a band gap equal to the photon energy ($|E_n - E_l| = \hbar w$) contributes to the response under linearly polarized light. It indicates that the shift current distributes mainly in some selective small areas in the momentum space. When the incident photon energy is sufficiently small, the response current only comes from the gap between two Weyl bands due to the energy selection rule. In the $\delta = \hbar/\tau \to 0$ limit (long relaxation time limit, which is valid for semiconductors and insulators), the summation over band m can be performed analytically via the first-order perturbation correction of the Bloch wave function [52]. In the end, we obtain the shift vector formula for the shift current density [22,52]. The shift vector directly connects the response photocurrent with a charge center shift between the valence and conduction bands, but is quite numerically unstable for a metallic system with a low-frequency driving field, due to the energy delta function and gauge fix of the Berry connection of valence and conduction bands, and is not suited to deal with scattering processes with a finite relaxation time. In a two-band approximation, the shift current response σ^a_{aa} ($a = x,y,z$) is zero as the velocity numerator N is real (here, $l = m$, $N = \langle l\vec{k}|\hat{v}_a|l\vec{k}\rangle|\langle n\vec{k}|\hat{v}_a|l\vec{k}\rangle|^2$), in which the velocity $v_a \equiv \langle l\vec{k}|\hat{v}_a|l\vec{k}\rangle$ is odd to $\vec{k}$ due to the time-reversal symmetry. Therefore, to properly calculate the shift current in real materials, one needs to use a multiband approach beyond the two-band approximation.

For circularly polarized light with a helicity-dependent term $\phi_{ab} = i$, the dispersive part $\mathrm{Re}(D_1D_2)$ [$\sim\frac{1}{(E_n-E_m)(E_n-E_l+\hbar\Omega)}$; note the relaxation time plays a minor role in CPGE] contributes to the response photocurrent. The absence of a δ function in $\mathrm{Re}(D_1D_2)$ indicates that there is no specific energy selection rule in the transition. Thus, in contrast to the concentrated distribution of the shift current, the CPGE distribution can be rather smeared out in momentum space. It also indicates that different transition pathways (real and virtual) contribute relatively equally to the photocurrent, assuming comparable numerators N. Given the large number of three-band virtual transitions, the virtual process might overwhelm the two-band direct process to induce the photocurrent.

To calculate the second-order photoconductivity in realistic compounds, we obtain the density functional theory (DFT) Bloch wave functions from the full-potential local-orbital program (FPLO) [56] within the generalized gradient

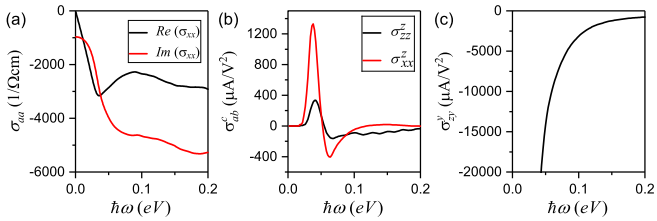

FIG. 2. Photon energy dependence of (a) optical conductivity, (b) shift current conductivity under linearly polarized light, and (c) circular photogalvanic conductivity.

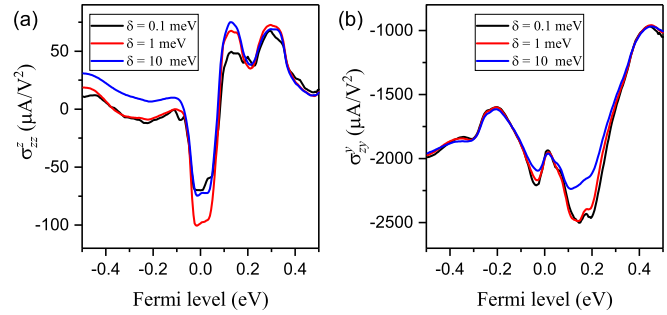

FIG. 3. Fermi level dependence of (a) shift current and (b) circular photogalvanic conductivity at $\hbar\omega = 120$ meV. Each line shows the results for different relaxation times.

approximation (GGA) [57]. By projecting the Bloch wave functions onto Wannier functions, we obtain a tight-binding Hamiltonian with 32 bands, which we use for an efficient evaluation of the photocurrent. For the integrals of Eq. (1), the Brillouin zone (BZ) was sampled by k grids from $200 \times 200 \times 200$ to $960 \times 960 \times 960$. Satisfactory convergence was achieved for a k grid of size $240 \times 240 \times 240$ for all three compounds. Increasing the grid size to $960 \times 960 \times 960$ varied the conductivity by less than 5%.

Realistic materials. The material TaAs belongs to the point group $4mm$, and has mirror reflections in the x and y directions. Due to the mirror symmetries, the nonzero conductivity elements are limited to the ones with an even number of x and y, i.e., σ^z_{xx},σ^z_{yy},σ^z_{zz},$\sigma^y_{zy}(\sigma^y_{yz})$,$\sigma^x_{zx}(\sigma^x_{xz})$. In addition, the 4_2 screw rotation symmetry about the z axis gives the relation $\sigma^z_{xx} = \sigma^z_{yy}$,$\sigma^y_{zy} = \sigma^x_{zx}$. Therefore, only three independent elements exist, i.e., σ^z_{xx}, σ^y_{zy}, and σ^z_{zz}. For the shift current, all three elements matter. For CPGE, only σ^y_{zy} is relevant.

Since the photocurrent response arises from both real and virtual band transitions, it generally has a strong dependence on the incident photon energy. As we are starting from a relaxation time approximation, the incident photon energy in our calculation should be above 5 meV (for the typical relaxation time $\delta = \frac{\hbar}{\tau}$ for metallic systems, we use $\delta = 10$ meV in our calculations). Thus, we focus on the midinfrared region from 20 to 200 meV, which contains the transitions between the Weyl bands. In TaAs, two groups of type-I Weyl nodes exist: (1) four pairs of WPs, noted as W_1, on the $k_z = 0$ plane with energy -23 meV, and (2) eight pairs of WPs, noted as W_2, out of the $k_z = 0$ plane with energy 14 meV. The shift current shown in Fig. 2 has a strong peak at a photon energy $\hbar\omega = 40$ meV, around twice the energy of in-plane Weyl nodes, and is almost zero below the Weyl node energy scale in our calculation. This is explained by real transitions from band n to band l in Fig. 1: The photocurrent is nonzero only when $E_l(\vec{k}) > 0$, $E_n(\vec{k}) < 0$, $E_l(\vec{k}) - E_n(\vec{k}) = \hbar\omega$, and increases when $\hbar\omega$ is decreasing because of the $\frac{1}{\omega^2}$ in the prefactor of Eq. (1).

For the photon energy dependence of CPGE, the $1/(\hbar\omega)^2$ behavior is observed in the region where our approach is valid. Since the energy denominator $\mathrm{Re}(D_1 D_2)$ is the dispersive part of the second-order optical response, the complex integral is nearly unchanged in the low-frequency regime, leading to a $1/(\hbar\omega)^2$ dependence due to the prefactor of Eq. (1).

Effect of disorders and fluctuations. Next, we discuss the effect of temperature and impurity scattering on photocurrent generation. In our calculation, the effects of disorder and fluctuations are taken into account by the constant relaxation time τ, which is not considered in the shift vector formalism [22,23]. Since the distribution of shift current in momentum space is quite concentrated around the Weyl nodes, the constant relaxation time would lead to almost the same results compared with more realistic momentum-dependent relaxation times. Another possible effect on the conductivities comes from the change in the electron distribution. However, since most of the experiments are carried out at low temperature [$k_B T = 4.3$ meV ($T = 50$ K), which is comparable to δ and much smaller than the frequency of light], we expect the temperature change in the Fermi-Dirac distribution function does not significantly modify the conductivity.

Figure 3 shows the chemical potential dependence of the shift current and CPGE, calculated with different relaxation times. As shown in Fig. 3, both terms show only a small dependence on the relaxation time. For the shift current σ^z_{zz}, the response current is maximized when the Fermi level is adjusted around the Weyl node energy, and changes only by 20% even if the relaxation time is changed by a factor of 100. For the CPGE σ^z_{yz} curve, the response current is almost unchanged at the charge neutrality point, and does not show a strong dependence on the Weyl node energy level.

Two- and three-band processes. For a given valence band n and conduction band l, the CPGE and shift current should sum over the real transition [$n \to l$, $l = m$ in Eq. (1)] and also the virtual transitions [$n \to m \to l$, $l \neq m$ in Eq. (1)] for all third bands m. To understand the importance of virtual transitions, here, we separate the two- and three-band process contributions for the response at an incident photon energy $\hbar\omega = 120$ meV, to investigate which one is more essential in the photocurrent generation.

As shown in Fig. 4(a), the three-band part of CPGE σ^y_{zy} is 1825 μA/V^2, while the two-band part is only 75 μA/V^2 at the charge neutrality point. We obtain $J_y = 1.2 \times 10^{-4}$ A with only two-band transitions in our method, which matches well with the theoretically calculated result 1.015×10^{-4} A in Ref. [46] via an effective two-band model.

Similarly, for the entire range of the Fermi level we calculated, a large contribution to the photocurrent comes from the three-band processes. The distribution of the three-band contribution for σ^y_{zy} is quite dispersed in momentum space, in contrast to the two-band part concentrating around the WPs. In total magnitude, the two-band process is ten times smaller than the three-band process. Taking a closer look at the small

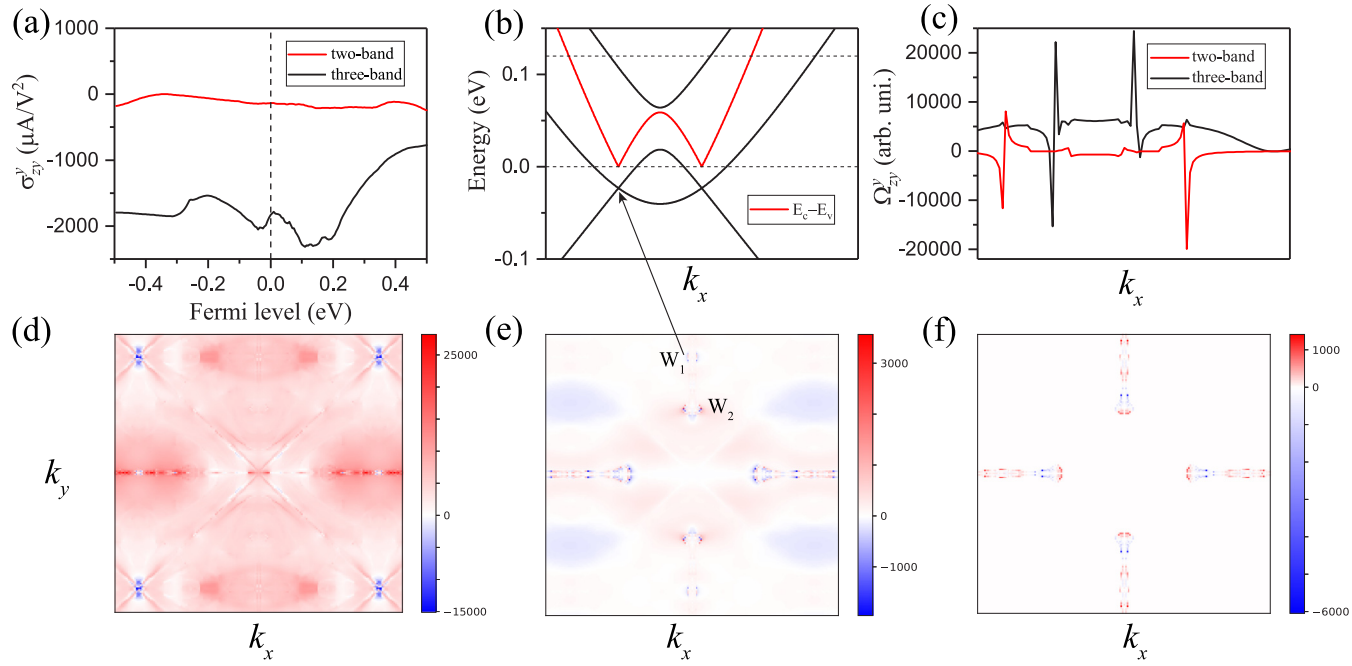

FIG. 4. (a) Three-band and two-band part of the Fermi-level-dependent CPGE σ^y_{zy} at $\hbar\omega = 120$ meV. (b) Band structure in the k_x direction across the w_1 Weyl node. (c) Three-band and two-band contribution of Ω^y_{zy} (CPGE σ^y_{zy} in momentum space) throughout the same k path as (b); the blue curve is the band gap between the valence and conduction band. (d) Three-band part of σ^y_{zy}(CPGE) in the first Brillouin zone. (e) Two-band part of σ^y_{zy}(CPGE) in the first Brillouin zone. (f) σ^z_{zz}(shift) in the first Brillouin zone.

area around the W_1 WPs, the two-band part solely comes from $E_v(\vec{k}) - E_c(\vec{k}) = 120$ meV, which is the direct transition between two Weyl bands, while the three-band contribution stays almost uniformly in the momentum space, implying that virtual transitions have a larger contribution than the real transitions.

It should be stressed that the shift current σ^z_{zz} is purely a three-band process, as we have analyzed according to Eq. (1) and have also confirmed in numerical calculations. Therefore, it is necessary to include a third band for the evaluation of the photocurrent $\vec{J}$ parallel to the electric field $\vec{E}$. In the momentum space distribution of the shift current σ^z_{zz}, the nonzero part is concentrated around the WPs, which shows the absorptive nature of the shift current. Thus, we can conclude that the shift current in the Weyl system comes from the interplay of Weyl nodes and third trivial bands when the incident photon energy is at the same scale of the energy of the Weyl nodes.

Discussion. We have systematically studied the photocurrent response both for linearly and circularly polarized light in type-I WSM TaAs, and show that the shift current spectrum has a strong dependence on the Weyl point energy, while CPGE shows a $1/(\hbar\omega)^2$ behavior in the midinfrared regime, when the incident photon energy is larger than the smearing energy. Comparing our calculated results with recent photocurrent experiments, we observe that the CPGE experiment of TaAs [46] measured σ^y_{zy}(CPGE) with an incident photon energy $\hbar\omega = 120$ meV. Our calculated σ^y_{zy} is 1900 μA/V^2, and gives a photocurrent $J_y = 2.1 \times 10^{-3}$ A under the experimental laser power. Taking into account a scaling factor 10^{-4} determined in experiment [46] and other unspecified decay channels, our results agree well with the experimental value of 40×10^{-9} A. The calculated shift current J_y is 8×10^{-5} A in this setup (4% of the photocurrent from circularly polarized light), which may possibly explain why the shift current was neglected in Ref. [46] that focused on the CPGE.

Recently, the shift current was experimentally studied in TaAs [48] and σ^z_{xx}, σ^z_{zz}, and σ^x_{zx} were measured at a photon energy $\hbar\omega = 117$ meV, which is at least an order of magnitude larger than previously measured materials [e.g., σ^z_{zz}(shift) = 0.013 μA/V^2 in $BaTiO_3$ with visible light [22,58]]. Our calculated σ^x_{zx}(shift) is 79 μA/V^2, in good agreement with the experimental result of $\sigma^x_{zx} = 26$ μA/V^2.

Apart from the above fixed photon energy experiments, it would be interesting to investigate the frequency-dependent photocurrent both for circularly and linearly polarized light, to verify the $1/(\hbar\omega)^2$ dependence of CPGE and the peak of the shift current for $\hbar\omega$ being around twice that of the WP (W_1) energy.

In addition, the calculated second-harmonic (SH) susceptibility χ^z_{zz} and the ratio of χ^x_{zx}/χ^z_{zz} are 6200 pm/V and 0.3, respectively, which are quite close to the measured values 7200 pm/V and 0.031 at low temperature [45].

Here, we present the generalized formulism for second-harmonic generation (SHG),

$$\sigma^c_{ab} = \frac{|e|^3}{8\pi^3\omega^2}\mathrm{Re}\Bigg\{\phi_{ab}\sum_{\Omega=\pm\omega}\sum_{l,m,n}\int_{\mathrm{BZ}} d^3k(f_l - f_n) \times \frac{\langle n\vec{k}|\hat{v}_a|l\vec{k}\rangle\langle l\vec{k}|\hat{v}_b|m\vec{k}\rangle\langle m\vec{k}|\hat{v}_c|n\vec{k}\rangle}{(E_n - E_m - 2\hbar\Omega - i\delta)(E_n - E_l + \hbar\Omega - i\delta)}\Bigg\}. \tag{3}$$

The second-harmonic susceptibility is given by $\chi^c_{ab} = \sigma^c_{ab}/2i\omega\epsilon_0$. The SHG has a similar behavior as the shift current,

and we will analyze the photon-energy-dependent spectrum in future work.

In summary, we have developed a first-principles multiband approach to determine the photocurrent response from linearly and circularly polarized light. We have established that the virtual transitions from Weyl bands to trivial bands play an essential role in the photocurrent generation process. In general, our method is also useful to study the nonlinear optical responses in ordinary metallic and insulating materials.

Acknowledgments. We thank N. Ogawa and T. Morimoto for helpful discussions. C.F. acknowledges the European Research Council (ERC) Advanced Grant (No. 742068) "TOPMAT". Y.Z., C.F., and J.v.d.B. acknowledge the German Research Foundation (DFG) SFB 1143. Y.Z. acknowledges the computing time of the Juelich supercomputer facilities. B.Y. is supported by a research grant from the Benoziyo Endowment Fund for the Advancement of Science.

[1] H. Weyl, Z. Phys. A: Hadrons Nucl. **56**, 330 (1929).
[2] H. Weng, C. Fang, Z. Fang, B. A. Bernevig, and X. Dai, Phys. Rev. X **5**, 011029 (2015).
[3] S.-M. Huang, S.-Y. Xu, I. Belopolski, C.-C. Lee, G. Chang, B. Wang, N. Alidoust, G. Bian, M. Neupane, C. Zhang, S. Jia, A. Bansil, H. Lin, and M. Z. Hasan, Nat. Commun. **6**, 8373 (2015).
[4] B. Q. Lv, H. M. Weng, B. B. Fu, X. P. Wang, H. Miao, J. Ma, P. Richard, X. C. Huang, L. X. Zhao, G. F. Chen, Z. Fang, X. Dai, T. Qian, and H. Ding, Phys. Rev. X **5**, 031013 (2015).
[5] S.-Y. Xu, I. Belopolski, N. Alidoust, M. Neupane, G. Bian, C. Zhang, R. Sankar, G. Chang, Y. Zhujun, C.-C. Lee, H. Shin-Ming, H. Zheng, J. Ma, D. S. Sanchez, B. Wang, A. Bansil, F. Chou, P. P. Shibayev, H. Lin, S. Jia, and M. Z. Hasan, Science **349**, 613 (2015).
[6] L. X. Yang, Z. K. Liu, Y. Sun, H. Peng, H. F. Yang, T. Zhang, B. Zhou, Y. Zhang, Y. F. Guo, M. Rahn, D. Prabhakaran, Z. Hussain, S. K. Mo, C. Felser, B. Yan, and Y. L. Chen, Nat. Phys. **11**, 728 (2015).
[7] X. G. Wan, A. M. Turner, A. Vishwanath, and S. Y. Savrasov, Phys. Rev. B **83**, 205101 (2011).
[8] G. E. Volovik, *The Universe in A Helium Droplet* (Clarendon, Oxford, U.K., 2003).
[9] S. Murakami, New J. Phys. **9**, 356 (2007).
[10] A. A. Burkov, M. D. Hook, and L. Balents, Phys. Rev. B **84**, 235126 (2011).
[11] P. Hosur and X. L. Qi, C. R. Phys. **14**, 857 (2013).
[12] B. Yan and C. Felser, Annu. Rev. Condens. Matter Phys. **8**, 337 (2017).
[13] N. P. Armitage, E. J. Mele, and A. Vishwanath, Rev. Mod. Phys. **90**, 015001 (2018).
[14] N. Nagaosa, J. Sinova, S. Onoda, A. H. MacDonald, and N. P. Ong, Rev. Mod. Phys. **82**, 1539 (2010).
[15] D. Xiao, M.-C. Chang, and Q. Niu, Rev. Mod. Phys. **82**, 1959 (2010).
[16] H. B. Nielsen and M. Ninomiya, Nucl. Phys. B **185**, 20 (1981).
[17] H. B. Nielsen and M. Ninomiya, Phys. Lett. B **130**, 389 (1983).
[18] J. Xiong, S. K. Kushwaha, T. Liang, J. W. Krizan, M. Hirschberger, W. Wang, R. J. Cava, and N. P. Ong, Science **350**, 413 (2015).
[19] J. Gooth, A. C. Niemann, T. Meng, A. G. Grushin, K. Landsteiner, B. Gotsmann, F. Menges, M. Schmidt, C. Shekhar, V. Suß, R. Hühne, B. Rellinghaus, C. Felser, B. Yan, and K. Nielsch, Nature (London) **547**, 324 (2017).
[20] J. E. Moore and J. Orenstein, Phys. Rev. Lett. **105**, 026805 (2010).
[21] E. Deyo, L. E. Golub, E. L. Ivchenko, and B. Spivak, arXiv:0904.1917.
[22] S. M. Young and A. M. Rappe, Phys. Rev. Lett. **109**, 116601 (2012).
[23] J. E. Sipe and A. I. Shkrebtii, Phys. Rev. B **61**, 5337 (2000).
[24] T. Morimoto and N. Nagaosa, Sci. Adv. **2**, e1501524 (2016); note that the two-band model of the shift current in this paper does not contradict the conclusion in the present Rapid Communication. Their two-band model effectively takes into account the multiband effect through the momentum dependence of the interband matrix elements of the current, while we take the pure p/m_0 as the current operator.
[25] T. Choi, S. Lee, Y. J. Choi, V. Kiryukhin, and S.-W. Cheong, Science **324**, 63 (2009).
[26] S. Y. Yang, J. Seidel, S. J. Byrnes, P. Shafer, C. H. Yang, M. D. Rossell, P. Yu, Y. H. Chu, J. F. Scott, J. W. Ager III, L. W. Martin, and R. Ramesh, Nat. Nanotechnol. **5**, 143 (2010).
[27] I. Grinberg, D. V. West, M. Torres, G. Gou, D. M. Stein, L. Wu, G. Chen, E. M. Gallo, A. R. Akbashev, P. K. Davies, J. E. Spanier, and A. M. Rappe, Nature (London) **503**, 509 (2013).
[28] M. M. Vazifeh and M. Franz, Phys. Rev. Lett. **111**, 027201 (2013).
[29] P. Goswami, G. Sharma, and S. Tewari, Phys. Rev. B **92**, 161110 (2015).
[30] M. Kargarian, M. Randeria, and N. Trivedi, Sci. Rep. **5**, 12683 (2015).
[31] H. Ishizuka, T. Hayata, M. Ueda, and N. Nagaosa, Phys. Rev. Lett. **117**, 216601 (2016).
[32] H. Ishizuka, T. Hayata, M. Ueda, and N. Nagaosa, Phys. Rev. B **95**, 245211 (2017).
[33] P. Hosur, Phys. Rev. B **83**, 035309 (2011).
[34] I. Sodemann and L. Fu, Phys. Rev. Lett. **115**, 216806 (2015).
[35] C.-K. Chan, P. A. Lee, K. S. Burch, J. H. Han, and Y. Ran, Phys. Rev. Lett. **116**, 026805 (2016).
[36] T. Morimoto, S. Zhong, J. Orenstein, and J. E. Moore, Phys. Rev. B **94**, 245121 (2016).
[37] K. Taguchi, T. Imaeda, M. Sato, and Y. Tanaka, Phys. Rev. B **93**, 201202(R) (2016).
[38] F. de Juan, A. G. Grushin, T. Morimoto, and J. E. Moore, Nat. Commun. **8**, 15995 (2017).
[39] C.-K. Chan, N. H. Lindner, G. Refael, and P. A. Lee, Phys. Rev. B **95**, 041104 (2017).
[40] E. J. König, H. Y. Xie, D. A. Pesin, and A. Levchenko, Phys. Rev. B **96**, 075123 (2017).
[41] H. Rostami and M. Polini, Phys. Rev. B **97**, 195151 (2018).
[42] L. E. Golub, E. L. Ivchenko, and B. Z. Spivak, JETP Lett. **105**, 782 (2017).
[43] Y. Zhang, Y. Sun, and B. Yan, Phys. Rev. B **97**, 041101 (2018).
[44] X. Yang, K. Burch, and Y. Ran, arXiv:1712.09363.

[45] L. Wu, S. Patankar, T. Morimoto, N. L. Nair, E. Thewalt, A. Little, J. G. Analytis, J. E. Moore, and J. Orenstein, Nat. Phys. **13**, 350 (2017).
[46] Q. Ma, S.-Y. Xu, C.-K. Chan, C.-L. Zhang, G. Chang, Y. Lin, W. Xie, T. Palacios, H. Lin, S. Jia, *et al.*, Nat. Phys. **13**, 842 (2017).
[47] K. Sun, S.-S. Sun, L.-L. Wei, C. Guo, H.-F. Tian, G.-F. Chen, H.-X. Yang, and J.-Q. Li, Chin. Phys. Lett. **34**, 117203 (2017).
[48] G. B. Osterhoudt, L. K. Diebel, X. Yang, J. Stanco, X. Huang, B. Shen, N. Ni, P. Moll, Y. Ran, and K. S. Burch, arXiv:1712.04951.
[49] S. Lim, C. R. Rajamathi, V. Süß, C. Felser, and A. Kapitulnik, arXiv:1802.02838.
[50] Z. Ji, G. Liu, Z. Addison, W. Liu, P. Yu, H. Gao, Z. Liu, A. M. Rappe, C. L. Kane, E. J. Mele, *et al.*, arXiv:1802.04387.
[51] W. Kraut and R. von Baltz, Phys. Rev. B **19**, 1548 (1979).
[52] R. von Baltz and W. Kraut, Phys. Rev. B **23**, 5590 (1981).
[53] N. Kristoffel and A. Gulbis, Z. Phys. B: Condens. Matter **39**, 143 (1980).
[54] J. Železný, H. Gao, A. Manchon, F. Freimuth, Y. Mokrousov, J. Zemen, J. Mašek, J. Sinova, and T. Jungwirth, Phys. Rev. B **95**, 014403 (2017).
[55] Y. Zhang, Y. Sun, H. Yang, J. Železný, S. P. P. Parkin, C. Felser, and B. Yan, Phys. Rev. B **95**, 075128 (2017).
[56] K. Koepernik and H. Eschrig, Phys. Rev. B **59**, 1743 (1999).
[57] J. P. Perdew, K. Burke, and M. Ernzerhof, Phys. Rev. Lett. **77**, 3865 (1996).
[58] A. Zenkevich, Y. Matveyev, K. Maksimova, R. Gaynutdinov, A. Tolstikhina, and V. Fridkin, Phys. Rev. B **90**, 161409 (2014).